Intra-operative Ultrasound hand-held Strain imaging for the Visualization of Ablations Produced in the liver with a Toroidal HIFU Transducer: First *In Vivo* Results

J Chenot[1], D Melodelima[1], W A N'Djin[1], Rémi Souchon[1], M Rivoire[1,2] and JY Chapelon[1]

Author affiliation:

[1]Inserm, U556, Lyon, F-69003, France; Université de Lyon, Lyon, F-69003, France.
[2]Centre Léon Bérard – Institut de Chirurgie Expérimentale, Lyon, F-69008, France.

E-Mail : jeremy.chenot@inserm.fr

Short title: Ultrasound Hand-held strain imaging for the visualisation of HIFU ablation: *in vivo* Results

ABSTRACT

The use of hand-held ultrasound strain imaging for intra-operative real-time visualization of HIFU ablations produced in the liver by a toroidal transducer was investigated. A linear 12 MHz ultrasound imaging probe was used to obtain radiofrequency signals. Using a fast cross-correlation algorithm, strain images were calculated and displayed at 60 frames/s, allowing the use of hand-held strain imaging intra-operatively. Fourteen HIFU lesions were produced in 4 pigs. Intra-operative strain imaging of HIFU ablations in the liver was feasible owing to the high frame rate. The correlation between dimensions measured on gross pathology and dimensions measured on B-mode images and on strain images were R = 0.72 and R = 0.94 respectively. The contrast between ablated and non-ablated tissue was significantly higher ($p<0.05$) in the strain images (22 dB) than in the B-mode images (9 dB). Strain images allowed equivalent or improved definition of ablated regions when compared with B-mode images. Real-time intra-operative hand-held strain imaging seems to be a promising complement to conventional B-Mode imaging for the guidance of HIFU ablations produced in the liver during an open procedure. These results support that hand-held strain imaging outperforms conventional B-mode ultrasound and could potentially be used for assessment of thermal therapies.

Key words: strain imaging, real-time, ultrasound, liver, HIFU, Elastography

INTRODUCTION

Imaging elastic properties of tissue for diagnosis of disease or for thermal treatment guidance is gaining attention since it is non-invasive and can provide new information regarding tissues. Among these techniques, elastography (strain imaging) allows the estimation of deformations in the medium when stress is applied (Ophir et al. 1991). The principle of strain imaging using ultrasound is the calculation of time delay between pre- and post-compression radiofrequency signals (RF), using a sliding window. Assuming a constant speed of sound in tissue, it is possible to estimate displacement. The strain image, called an elastogram, is obtained from the gradient of the displacement. Using this approach, many methods have been proposed for imaging the mechanical properties of tissues, and these may differ in a variety of ways, including the method used to stress the tissue, the nature of this stress (e.g. whether controlled stress or controlled displacement, and whether constant or time-varying), the property measured to describe the resulting tissue response, and the method used to measure this property (Muthupillai et al. 1995). In several applications, the load or displacement is applied externally to the surface of the tissue as in quasi-static compression (Doyley et al. 2001, Ophir et al. 1991, Plewes et al. 2000) or in dynamic vibration excitation (Muthupillai et al. 1995, Taylor et al. 2000). Internal physiologic motion has also been utilized, for cardiac (Varghese et al. 2003), liver (Kolen et al. 2004) and arterial strain imaging (Arnett et al. 1994). Acoustic radiation force has also been used to generate an internal load, non-invasively (Bercoff et al. 2004, Fatemi et al. 1999, Melodelima et al. 2007a, Melodelima et al. 2006, Nightingale et al. 2002).

Given previous demonstrations of stiffness contrast of thermal lesions created by radiofrequency ablation (Bharat et al. 2005, Fahey et al. 2008, Varghese et al. 2002), methods of imaging tissue elasticity may also hold promise for guiding and assessing ablation procedures, particularly for High Intensity Focused Ultrasound (HIFU) treatments (Kallel et al. 1999, Souchon et al. 2003). HIFU treatments are already guided by ultrasound scanner for numerous applications (Illing et al. 2006, Pichardo et al. 2008, Wu et al. 2004). Therefore, strain imaging could provide additional information to conventional B-mode imaging since elastograms can now be calculated in real-time (Pesavento et al. 2000, Zahiri-Azar et al. 2006, Zhu et al. 2002). In a previous study (Melodelima et al. 2007b) we have described the use of a toroidal high intensity focused ultrasound (HIFU) device for treating colorectal liver metastases. The selected approach for the toroidal HIFU treatment is surgical laparotomy. The

main advantage of performing the HIFU treatment during an open procedure is to make it possible to associate HIFU with hepatic resection. Indeed, hepatic resection, eventually combined with radiofrequency ablation (RFA) or cryosurgery ablation (CSA), is the gold standard in the treatment of colorectal liver metastases (Antoniou et al. 2007, Pawlik et al. 2003, Rivoire et al. 2002). Compared with RFA or CSA, HIFU, could represent a promising alternative for treating colorectal liver metastases. The principal interest in HIFU lies in the possibility of treating metastases for which the use of other destruction techniques is contra-indicated, notably for metastases located near a large vascular structure (Parmentier et al. 2009). This approach allows for treatment to all regions of the liver without penetrating the hepatic capsule. Furthermore, such an intra-operative approach ensures the protection of surrounding organs and eliminates the risk of lesions in other organs. Using this device, it was previously reported that the demarcation between ablated and non-ablated tissues was apparent using B-Mode images (Melodelima et al. 2009b).

In the current study, we hypothesize that ultrasound hand-held strain imaging may be useful in enhancing the guidance of ablations produced using this toroidal HIFU transducer during an open procedure for the treatment of liver metastases. Strain imaging may be useful during several stages of HIFU procedures, mainly intraprocedure guidance (demarcation between ablated and non-ablated tissues as well as detection of tumors not discovered on preoperative imaging) and postprocedure outcome assessment. Ultrasound hand-held strain imaging for guiding HIFU treatments in the liver during an open procedure has never been investigated. If successful, this imaging modality could also be used in the future to provide visualization of the ablated region for other thermal techniques like radiofrequency or cryosurgery. Experiments were conducted *in vivo* in porcine livers. Taking advantage of the open procedure approach that allows ultrasound imaging at high frequency (12 MHz), strain images were produced by manually and directly stressing the liver with an ultrasonic imaging probe. A fast algorithm allows calculating and displaying strain images at the frame rate of the ultrasound scanner. Strain imaging was implemented on a modified ultrasound scanner, allowing for combined real-time sonography/strain imaging. We present a feasibility study on use of the technique of combined hand-held sonography/strain imaging to detect HIFU ablations intra-operatively.

MATERIALS

A. Animals

Experiments were conducted *in vivo* in pig liver. There is no established liver tumor model in pigs due to the absence of porcine liver tumor cell lines. However, the pig is an ideal animal to study the different treatment options available for liver tumors because of its size and similar physiology to humans. Therefore, in this study, trials were conducted on normal liver tissues in 4 female Landrace pigs, 12-14 weeks old, with an average weight of 27.6 ± 1.5 kg [min. 26.2 – max. 29.5]. The experiments were conducted at the Institute of Experimental Surgery of the Léon Bérard Center, after local Institutional Review Board approval. These experiments conformed to the requirements of the local Office of Animal Experimentation and were in accordance with the legal conditions of the National Commission on Animal Experimentation. The animals were kept on-site seven days before the start of the experiments.

B. HIFU probe

The HIFU device was composed of a driving equipment similar to that previously reported (Melodelima et al. 2006) and a sterilized treatment probe also previously described (Melodelima et al. 2009b). Briefly, the ultrasound fields were generated using eight ultrasound emitters operating at a frequency of 3 MHz and distributed according to a toroidal geometry with a diameter of 70 mm and a radius of curvature of 70 mm. The use of a 3 MHz HIFU transducer is not typical for abdominal applications, which usually use lower frequencies to allow for application through the skin/subcutaneous fat. However the use of the device during an open procedure allows the use of a higher frequency. Using numerical simulations, the choice of 3 MHz was judged to be the best compromise between heat deposition and no cavitation effects.

Due to the toroidal shape of the transducer, the focal zone was slightly conical. The focal zone observed in the focal plane was a ring. The −6 dB beam axial focal length of the produced focal zone was 28.8 mm. The −6 dB outer diameters at the two extremities of the produced conical focal zone were 19.5 and 18.0 mm, respectively. These pressure fields were described in detail in a previous study (Melodelima et al. 2007b). The ablation zone (conical in shape)

induced in 40 seconds has a diameter of 2 cm, a major axis of 2.5 cm, and was placed at 7 cm from the emitting surface to enable treatment of deep regions in the liver. A 7.5 MHz ultrasound imaging probe (Vermon, Tours, France) was placed in the centre of the device and connected to a B-K HAWK 2102 EXL scanner (B-K Medical, Herlev, Denmark) to guide the treatment. The HIFU probe was brought into contact with the liver using a sterile ultrasound cooling and coupling liquid (Ablasonic®, Edap-Technomed, Vaulx en Velin, France) contained in a sterile polyurethane envelope (Civco, Kaloma, Iowa, USA). The software developed in our laboratory allows the user to target the HIFU treatment zone from a conventional B-mode image. The user interface allowed the visualization of the region to be coagulated by ultrasound exposure. The position of the HIFU focal region was superimposed on the ultrasound image. In this manner, the user can precisely position the treatment zone within the hepatic tissue.

C. Elastography system

Strain images were obtained using a linear 12 MHz ultrasound probe (Model 8805, B-K Medical, Herlev, Denmark) connected to a B-K ultrasound scanner (Hawk 2102 EXL, B-K Medical, Herley, Denmark). The scanner was modified in order to allow acquisition of RF lines by a computer (Dell Precision 690 Workstation with 2 quad-core Intel Xeon E5345 processors) via an analogue/digital converter (GaGe Octopus CS8327) having a sampling frequency of 40 MHz. A schematic diagram of the experimental apparatus is shown in figure 1.

METHODS

A. Treatment and imaging procedure

Twenty-four hours before treatment, the food intake of the animal was restricted with free access to water. Premedication was performed 30 minutes before anesthesia using an intramuscular injection of ketamine (Kétalar®, Parke-Davis, Courbevoie, France) at a dosage of 20 mg/kg. A catheter (Willy Rush, Waiblingen, Germany) was placed in an auricular vein. A dose of 5 mg/kg of Propofol (Diprivan®, AstraZeneca, Rueil Malmaison, France) was

administered just before intubation. Ventilation was performed with a Servo 900B® type respirator (Siemens Life Support Service, Solna, Sweden) at 10 L/min and at a frequency of 18 to 20 respiratory movements per minute with a 50% air/oxygen mix. Anesthesia was maintained using a slow intravenous injection of Propofol (20mg/kg/h) and sufentanil (10µg/kg/h; Sufenta®, Jassen-Cilag, Berchem, Belgique) in a continuous perfusion of physiological saline solution. Hydration was provided by an isotonic perfusion of physiological saline solution at 9%. The animals were monitored continuously by evaluating hemodynamic status and blood oxygen saturation.

A 25 cm median laparotomy was performed from the xyphoid process. Pads were placed below and on the sides of the liver and were utilized in order to protect adjacent organs from possible unwanted lesions. The HIFU probe was held by hand at the surface of the liver. The region to be treated was located using the 7.5 MHz integrated ultrasound imaging probe. Each HIFU exposure was performed during apnea to avoid liver movement. Apnea periods always began 5 seconds before sonication and lasted 45 seconds. The purpose of this maneuver was to limit the movements of the liver, which could have been deleterious to treatment quality. Fourteen HIFU ablations were performed using an underrated acoustic power of 50 watts, and the exposure duration was 40 seconds. The exposure conditions are derived from preliminary *in vivo* studies (Melodelima et al. 2009b). At the end of the treatment the laparotomy was closed in two planes. After the treatment, post-operative analgesia was administered to each animal by a fentanyl patch at a 100-µg dosage every three days (Durogesic ®, Janssen-Cilag, Berchem, Belgium).

B. Strain images acquisition

Imaging during the surgical intervention would of course have been of great interest. However, for this preliminary study, the imaging procedure was approved by our local institutional review board to be performed at the end of a protocol approved for the above described HIFU treatment. Therefore, strain images were acquired 21 days after the HIFU treatment, during a second open procedure. One advantage is that it allows a direct comparison between the images and gross pathology since lesions were examined just after the imaging procedure.

The animals were prepared as described above. After laparotomy, the 12 MHz ultrasound probe was housed in a sterile polyurethane envelope (Civco, Kaloma, Iowa, USA) and used to acquire strain images. Strain was induced manually by pushing and pulling the imaging probe

at the surface of the liver. The amplitude and speed of the displacement were adapted by the operator as a function of the strain results visualized in real-time. The liver was pre-compressed manually by about 1 – 3 mm to ensure good contact between the imaging probe and the organ. During the strain imaging procedure, the amplitude and speed of the axial displacement were adapted by the operator as a function of the strain images visualized in real-time. Axial displacements of less than 0.5 mm were applied around this initial position of the imaging probe to produce strain images that were judged satisfactory. The thickness of the livers used in this study was between 2 and 4 cm. Therefore the applied stress represents a maximal strain of 1% using the maximal scan depth of 5 cm used in this study. This value was a compromise between the stress that can be applied at the surface of the liver without damaging the organ or adjacent viscera and the quality of the resulting strain images.

Ultrasound data was captured continuously and strain images were processed and displayed in real-time. Displacement estimation was performed using a time-domain cross-correlation algorithm similar to that described by (Zahiri-Azar et al. 2006). Strain was estimated using the staggered strain estimator (Srinivasan et al. 2002). The displacement estimation (tracking) window length was set to 0.6 mm (approximately 4 pulse lengths) and the size of the strain estimation kernel ("staggering kernel") was increased until the subjective visibility of strain at the ablation location was maximized. A staggering kernel length of 0.9 mm was deemed satisfactory. The window shift was chosen as small as possible (0.3 mm) while still allowing the images to be produced at a speed of 60 frames per second (fps). The same values were used for processing all data sets.

Sonograms, correlation, displacements and strains fields were displayed simultaneously on the screen at a rate of 60 fps. Care was taken by visual observation of the real-time images during all acquisitions to minimize the lateral and elevational displacements (caused by transducer motion), thus optimizing correlation between pre and post compression RF images. When strain images were deemed satisfactory, the acquisition system was paused and a cine-loop containing the last 200 consecutive RF images was saved (corresponding to a recording time of 3.7 seconds). The diameter and the depth of all ablations were measured on strain images and B-mode images.

After the acquisition of the strain images, the pigs were euthanized by a single intravenous 0.3 ml/kg injection containing embutramide, mebezonium and tetracaine (T61®, Intervet, Beaucouze, France). A total hepatectomy was then done in order to visually inspect the ultrasound effects. The lesions were cut along the imaging axis. The diameter and the depth of

all ablations were measured so that their dimensions were defined by a boundary (defined as a lighter color) outlining the ablated region. It is known that the edge of the red tissue is really the boundary between the normal tissue and that treated by thermal ablation. This narrow transition from treated to normal tissue was previously described and confirmed by histological observations to be approximately 200 μm (Melodelima et al. 2009a, Vykhodtseva et al. 2006). Dimensions were measured using a caliper leading to an uncertainly of around 1 mm. The examiner measuring the dimensions of the ablations on gross pathology was different from the examiner measuring dimensions on B-Mode imaging and strains images. The two examiners were blinded to the results of each other.

C. Data analysis

Data are presented as mean ± standard deviation [min – max]. Pearson's correlation was used to determine the relationship between the dimensions of the lesions measured on gross pathology, strain images and sonograms. The quality of strain images was assessed by computing the contrast-to-noise ratio (CNRe) and the signal-to-noise ratio (SNRe), which were defined as follows (Chaturvedi et al. 1998):

$$CNR_e = \sqrt{\frac{2(\varepsilon_A - \varepsilon_T)^2}{\sigma_A^2 + \sigma_T^2}} \quad (1)$$

Where ε_A and ε_T represent the mean strain of the ablated zone and in the untreated tissues respectively, and σ_A^2 and σ_T^2 represent the variances in strain in the ablated zone and untreated tissues respectively.

$$SNR_e = \frac{\varepsilon_A}{\sigma_A} \quad (2)$$

Where ε_A and σ_A represent the mean strain and the standard deviation in the ablated zone. Contrast calculations were also performed using regions of interest (ROIs) that were selected both inside the ablated zone and in adjacent untreated tissues. The reason for choosing a location near the ablated zone for the untreated ROI is that visual contrast demarcation is generally made by the human eye for region located close to each other. ROI location was chosen by the consensus of two observers after examination of B-Mode and strain image data. ROIs within ablations were chosen to be as large as possible while confidently remaining

within ablation boundaries. For each data set, the ROIs used for B-mode and strain image contrast calculations were identical. Contrast was calculated using equation 3:

$$C = \left| 20 * \log \left(\frac{\varepsilon_A}{\varepsilon_T} \right) \right| \quad (3)$$

Where ε_A and ε_T are the mean B-mode or strain pixel magnitude inside the ablated and the untreated tissues, respectively. In the B-mode images, the HIFU ablations were seen as a hypoechoic region with a central hyperechoic zone. Therefore, three different contrast values were computed: (i) the contrast between untreated liver and the entire ablation zone, (ii) the contrast between the untreated liver and the central part of the ablation (hyperechoic zone) and (iii) the contrast between the untreated liver and the edges of the ablation (hypoechoic zone). Contrasts were compared using Student's t test. The significance level for all tests was fixed at $p < 0.05$.

RESULTS

Fourteen HIFU ablations were observed on sonograms and strain images. The mean diameter of ablations measured on gross pathology was 11.4 ± 3.3 mm [6.0 – 18.0] with a mean depth of 15.6 ± 6.2 mm [8.0 – 30.0]. The uncertainly of the measurement was around 1mm because of the graduation of the caliper. The correlation between the dimensions measured on strain images and those measured on gross pathology was R=0.94. The correlation between the dimensions measured on B-mode images and those measured on gross pathology was R=0.72. This value is consistent with our previous experiments with B-mode monitoring only (Melodelima et al. 2009b) where a coefficient R=0.67 was found. The correlation between the dimensions measured on strain images and on sonograms was 0.77. Figure 2(a) and figure 2(b) shows the correlation between the dimensions of the ablations measured on strain images, B-mode images and the actual dimensions measured on gross pathology.

The mean CNRe of the strain images was 11.4 ± 3.1 [7.7 – 18.2] with a mean SNRe of 2.8 ± 1.1 [1.4 – 4.7]. The mean contrast between the treated zone and the untreated zone was 22.0 ± 10.3 dB [9.1 – 40.6] in the strain images versus 9.3 ± 5.5 dB [0.1 – 20.0] in B-mode images (when the entire ablation appearing in B-mode images was taken into account). On B-mode images the mean contrast between the treated zone and the untreated zone was 3.5 ± 3.0 dB [0.0 – 10.0] when only the hyperechoic zone of the lesion was taken into account, and 14.4 ±

5.5 dB [1.6 – 21.3] when only the hypoechoic zone of the lesion was taken into account. All these results are summarized in table 1. Relationships between contrasts measured on strain images and those measured on sonograms are presented in figure 3. The contrast of the entire lesion observed on strain images was significantly higher when compared to the different contrast observed on sonograms ($p<0.05$ in all cases).

Fig. 4a shows an example of a single ablation produced in 40 seconds using the toroidal device and imaged using conventional B-Mode imaging. Figure 4(b) shows the corresponding strain image. In figure 4(a), the ablation appears as a hypoechoic cone containing a conical hyperechoic zone. These features are typical of HIFU ablations created in the liver with the toroidal device (Melodelima et al. 2009b). The strain images display the treated zones with a more homogenous appearance (figure 4(b)) and corresponding well to the actual dimensions of the ablation (figure 4(c)).

In two strain images, it was possible to observe the presence of a blood vessel (figure 5(a)). During the compression cycles, the veins were flattened and then dilated. They were associated with decorrelation and significant displacement estimation error. This phenomenon could be observed before and after an ablation (Fan et al. 2007). These random displacement estimates induced very visible zones (artefactual strain) in strain images. This particularity can be utilized, for example, to verify the presence of blood vessels before a HIFU ablation is created. In addition, two abscesses caused by ablations on biliary tracts were also imaged by hand-held strain imaging (figure 5(b)).

In two cases, strain images allowed more accurate evaluation of the ablation dimensions. In these two cases, the HIFU ablation was inhomogenous. For example, Figure 6 shows an ablation divided in two color zones and different appearances, corresponding to a zone where the activity of cavitation and/or ebullition seems to have been significant. Gross pathology - figure 6(c) - shows cavities and dark zones in the treated area. In the corresponding B-mode image (figure 6(a)), only half of the HIFU ablation was visible. The sonogram shows two hypo and hyper echogenic zones with a slight shadowing behind, but does not match the dimensions measured on gross pathology. In the strain image (fig. 6(b)), it is possible to distinguish two regions: a cone formed by the dark zone supported by a triangular point. In that particular case, the strain images showed better correspondence with the shape observed on gross pathology.

DISCUSSION

Intra-operative ultrasound hand-held strain imaging of HIFU ablation in the liver was feasible. Combined hand-held sonography/strain imaging is a straightforward imaging protocol that allows for the strengths of both modalities to be used in a highly complementary manner. Real-time hand-held sonography/strain imaging was particularly well-suited for assessing intra-operative HIFU ablation and good correspondence was found between measurements from pathology and strain imaging. Thus, this approach may provide additional relevant information during HIFU treatments in the liver during an open procedure without sacrificing the cost, convenience and portability benefits of conventional ultrasound monitoring. In this preliminary study, the imaging procedure could only be performed 21 days after the HIFU treatment. Nevertheless, we envision that the method will be feasible during or immediately after ablation. For this purpose, future work will be conducted with the ultrasound imaging probe integrated in the HIFU device.

Although the hand-held method used does not allow compressions to be as reproducible as the ones produced using motorized arms, the real-time display allowed the operator to visualize the effects of probe positioning and to adjust the strength and speed of axial compression in real-time. In addition, the operator could simultaneously visualize the B-mode image, the displacement, the correlation and the strain images.

The key elements to successful scanning were fast frame rate acquisition (60 fps), and real-time visual feedback of B-mode and strain images that guide the probe positioning and compression direction (Chandrasekhar et al. 2006, Hall et al. 2003). More than the overlap, the frame rate is the most important factor for the quality of strain images. In our initial experiments (unpublished) we used a slower system running at 8 strain images per second. This frame rate was too slow for hand-held strain imaging in the liver due to high sensitivity to motion artifacts and also to axial displacements that were produced too rapidly. The threshold to have acceptable strain images seems to be at least of 20-30 images/s (Chandrasekhar et al. 2006, Hall et al. 2003) but further studies are required to thoroughly evaluate this limit. In this study, a frame rate of 60 fps allowed the operator to see the effect of axial compressions immediately and to adjust the induced displacement to improve the quality of the resulting strain images. Additionally, high frame rate minimized the deleterious effects of movements (breathing and swiping of the probe) on strain images quality. At 60 fps, the effect respiratory motions were negligible and the resulting strain images were due to the

stress applied by the probe at the surface of the liver. Faster movements, such as the ones caused by cardiac activity were localized around veins. The induced strain was about 5% and was localized 1 mm around the vessel. This has not compromise the strain imaging of HIFU ablations.

During compression of a non-homogenous medium, the different mediums are displaced in a non-uniform manner, leading to a phenomenon of a border effect between the mediums. This effect is visible as a discontinuity in the strain images. It allows the operator to visualize the ablations even if the elasticity of the ablation is close to the elasticity of the untreated liver. Indeed, in this study, there was one case were the HIFU ablation contained two zones of different elasticity. One was close to the untreated tissues (Figure 6). Based on a discontinuity visible in the corresponding strain images, it was possible to estimate correctly the dimensions of the ablation. At the opposite, it was not possible to determine the dimension of this ablation on B-Mode images. However this is a very specific and illustrating case and no definitive conclusions can be drawn from this example. In some cases, biliary ducts were ablated by the HIFU exposure, creating abscesses. The results of our study show that the elasticity of abscesses was comparable to that of the liver causing the CNRe of these strain images to be very low. Nevertheless, it was possible to image abscesses due to the edge effect previously described. The displacement images were continuous within the liver and within the abscess, with a characteristic discontinuity at the frontier. The contour of the abscess was more rigid compared with the liver, allowing the abscesses to appear on strain images.

In the past, *in vitro* experiments conducted by other investigators have shown that tissue damage induced by high-intensity focused ultrasound in excised canine liver specimens reveals high correlation (R^2=0.93) between elastographic and gross pathological measurements (Righetti et al. 1999). Our results show that high correlation (R=0.94, i.e. R^2=0.88) can be obtained as well but under *in vivo* conditions. The sonographic contrast between the untreated liver and the zones treated by HIFU allowed satisfactory identification of the ablations boundary in sonograms (R=0.72). Measurements performed on strain images showed a superior agreement with pathology (R=0.94).

In two cases, the sizes of ablations were larger than the others (Fig. 2). Previous studies shown that such dimensions (about 30mm) are usual (Melodelima et al. 2009b) and created in deeper liver regions. The correlation coefficients obtained when these two points are excluded were R=0.87 for strain images and R=0.80 for B-Mode images. Hence the inclusion/exclusion of these particular points did not significantly affect correlation. Regarding correlation results

it is noteworthy that the dispersion is less important for the measurements made using strain images. This can be explain by the fact that lesion boundary are visible more precisely on strain images.

Despite the limited number of samples, this study demonstrated that in some cases strain images can allow visualization of the treated zone with better accuracy, and particularly with a more homogenous contrast. Therefore, with combined hand-held sonography/strain imaging, HIFU ablation could be guided with ultrasound, eventually using real-time strain imaging when increased contrast or further information about the treated region are required. This method would likely increase operator confidence in assessing the ablation zone, compared to the use of B-Mode images alone. This combined approach seems promising and has also been suggested for the guidance and assessment of liver radiofrequency ablation with acoustic radiation force elastography (ARFI) (Fahey et al. 2008).

Due to the thickness of porcine liver (2 – 4 cm), ablations produced with this device generally extend from the surface to the bottom of the liver as previously described (Melodelima et al. 2009a). As a consequence, most HIFU lesions imaged in this study were directly in contact with the imaging probe. Human liver is thicker and it is expect that HIFU lesions will be deeper, most often behind a superficial untreated area. In such circumstances the HIFU lesions would be totally surrounded by soft untreated tissues. This should reinforce the contrast of the ablated area (Doyley et al. 2000). Hence we hypothesize that under these conditions, the quality of the imaging results would be similar or better. However, future clinical studies will need to be conducted to confirm the validity of this hypothesis.

Another limitation in this study is the relatively low SNRe compared with *in vitro* studies assessing relative stiffness of lesions created using high intensity focused ultrasound (HIFU) in the liver (Kallel et al. 1999). This was expected because of unwanted displacements encountered *in vivo*. In addition to the above mentioned breathing movements, the surface of the liver was not flat and the probe can slightly slide inducing lateral displacement during the applied axial compression.

In order to propose a therapeutic method that uses HIFU and adapted to the treatment of colorectal liver metastases the treatment was performed during an open procedure. This choice allowed associating the HIFU destruction technique with hepatic resection, which appears to be the best current strategy in curative treatment methods for liver metastases. Moreover, general anesthesia makes it possible to use apnea in order to create precise HIFU ablation in the liver. The intra-operative approach has also been suggested for radiofrequency

ablation (RFA) and cryosurgery (CSA). Therefore the imaging results presented here could also be used for RFA or CSA. Nevertheless, extracorporeal use of HIFU is possible as has been clinically demonstrated for other disease (Illing et al. 2005, Kennedy et al. 2004) and future work will concentrate on the potential of high frame rate for hand-held extracorporeal elastography.

In conclusion, we have presented initial results from an *in vivo* study investigating the performance of combined hand-held sonography/strain imaging in real-time for use with an intra-operative toroidal HIFU device developed for the treatment of liver metastases in conjunction with surgery. Initial results demonstrate the feasibility of this application. Real-time hand-held strain imaging allowed accurate measurement of the lesion dimensions, and was a useful complement to conventional sonograms. Further investigation is required to determine the full potential of intra-operative ultrasound strain imaging for visualizing tumor masses and the zones of the tumors that are effectively treated. Our results suggest that strain imaging may also provide useful information for the guidance of other thermal-based procedures (RF ablation and cryotherapy)

ACKNOWLEDGMENT

The authors wish to thank the staff of the laboratory for experimental surgery for their aid in the animal study. This work was supported by funding from the Cancéropôle Lyon Auvergne Rhône Alpes (PDC 2006.4.8), EDAP TMS (N° EDAP 88513 B45) and by NIH/NIBIB Program Project Grant P01-EB-02105 to the University of Texas Health Science Center at Houston.

REFERENCES

Antoniou A., Lovegrove R. E., Tilney H. S., Heriot A. G., John T. G., Rees M., Tekkis P. P. and Welsh F. K. 2007 Meta-analysis of clinical outcome after first and second liver resection for colorectal metastases *Surgery* **141** 9-18.

Arnett D. K., Evans G. W. and Riley W. A. 1994 Arterial stiffness: a new cardiovascular risk factor? *Am J Epidemiol* **140** 669-682.

Bercoff J., Tanter M. and Fink M. 2004 Supersonic shear imaging: a new technique for soft tissue elasticity mapping *IEEE Trans Ultrason Ferroelectr Freq Control* **51** 396-409.

Bharat S., Techavipoo U., Kiss M. Z., Liu W. and Varghese T. 2005 Monitoring stiffness changes in lesions after radiofrequency ablation at different temperatures and durations of ablation *Ultrasound Med Biol* **31** 415-422.

Chandrasekhar R., Ophir J., Krouskop T. and Ophir K. 2006 Elastographic image quality vs. tissue motion in vivo *Ultrasound Med Biol* **32** 847-855.

Chaturvedi P., Insana M. F. and Hall T. J. 1998 Testing the limitations of 2-D companding for strain imaging using phantoms *IEEE Trans Ultrason Ferroelectr Freq Control* **45** 1022-1031.

Doyley M. M., Bamber J. C., Fuechsel F. and Bush N. L. 2001 A freehand elastographic imaging approach for clinical breast imaging: system development and performance evaluation *Ultrasound Med Biol* **27** 1347-1357.

Fahey B. J., Nelson R. C., Hsu S. J., Bradway D. P., Dumont D. M. and Trahey G. E. 2008 In vivo guidance and assessment of liver radio-frequency ablation with acoustic radiation force elastography *Ultrasound Med Biol* **34** 1590-1603.

Fan L., Freiburger P., Lowery C. and Milkowski A. in *Sixth International Conferenceon the Ultrasonic Measurement and Imaging of Tissue Elasticity*© 68 (Santa Fe, New Mexico, USA, 2007).

Fatemi M. and Greenleaf J. F. 1999 Vibro-acoustography: an imaging modality based on ultrasound-stimulated acoustic emission *Proc Natl Acad Sci U S A* **96** 6603-6608.

Hall T. J., Zhu Y. and Spalding C. S. 2003 In vivo real-time freehand palpation imaging *Ultrasound Med Biol* **29** 427-435.

Illing R. O., Kennedy J. E., Wu F., ter Haar G. R., Protheroe A. S., Friend P. J., Gleeson F. V., Cranston D. W., Phillips R. R. and Middleton M. R. 2005 The safety and feasibility of extracorporeal high-intensity focused ultrasound (HIFU) for the treatment of liver and kidney tumours in a Western population *Br J Cancer* **93** 890-895.

Illing R. O., Leslie T. A., Kennedy J. E., Calleary J. G., Ogden C. W. and Emberton M. 2006 Visually directed high-intensity focused ultrasound for organ-confined prostate cancer: A proposed standard for the conduct of therapy *BJU Int* **98** 1187-1192.

Kallel F., Stafford R. J., Price R. E., Righetti R., Ophir J. and Hazle J. D. 1999 The feasibility of elastographic visualization of HIFU-induced thermal lesions in soft tissues. Image-guided high-intensity focused ultrasound *Ultrasound Med Biol* **25** 641-647.

Kennedy J. E., Wu F., ter Haar G. R., Gleeson F. V., Phillips R. R., Middleton M. R. and Cranston D. 2004 High-intensity focused ultrasound for the treatment of liver tumours *Ultrasonics* **42** 931-935.

Kolen A. F., Miller N. R., Ahmed E. E. and Bamber J. C. 2004 Characterization of cardiovascular liver motion for the eventual application of elasticity imaging to the liver in vivo *Phys Med Biol* **49** 4187-4206.

Melodelima D., Bamber J. C., Duck F. A. and Shipley J. A. 2007a Transient elastography using impulsive ultrasound radiation force: a preliminary comparison with surface palpation elastography *Ultrasound Med Biol* **33** 959-969.

Melodelima D., N'Djin W A., Favre-Cabrera J., Parmentier H., Rivoire M. and Chapelon J. Y. 2009a Thermal ablation produced using a surgical toroidal high-intensity focused ultrasound device is independent from hepatic inflow occlusion *Phys Med Biol* **54** 6353-6368.

Melodelima D., N'Djin W. A., Parmentier H., Chesnais S., Rivoire M. and Chapelon J. Y. 2009b Thermal ablation by high-intensity-focused ultrasound using a toroid transducer increases the coagulated volume. Results of animal experiments *Ultrasound Med Biol* **35** 425-435.

Melodelima D., N'Djin W. A., Parmentier H., Chesnais S., Rivoire M. and Chapelon J.-Y. 2007b Ultrasound surgery with a toric transducer allows the treatment of large volumes over short periods of time *Applied Physics Letters* **91** 1-3.

Melodelima D., Salomir R., Mougenot C., Moonen C. and Cathignol D. 2006 64-element intraluminal ultrasound cylindrical phased array for transesophageal thermal ablation under fast MR temperature mapping: an ex vivo study *Med Phys* **33** 2926-2934.

Muthupillai R., Lomas D. J., Rossman P. J., Greenleaf J. F., Manduca A. and Ehman R. L. 1995 Magnetic resonance elastography by direct visualization of propagating acoustic strain waves *Science* **269** 1854-1857.

Nightingale K., Bentley R. and Trahey G. 2002 Observations of tissue response to acoustic radiation force: opportunities for imaging *Ultrason Imaging* **24** 129-138.

Ophir J., Cespedes I., Ponnekanti H., Yazdi Y. and Li X. 1991 Elastography: a quantitative method for imaging the elasticity of biological tissues *Ultrason Imaging* **13** 111-134.

Parmentier H., Melodelima D., N'Djin W. A., Chesnais S., Chapelon J.-Y. and Rivoire M. 2009 High-intensity focused ultrasound ablation for the treatment of colorectal liver metastases during an open procedure: study on the pig *Ann Surg* **249** 129-136.

Pawlik T. M., Izzo F., Cohen D. S., Morris J. S. and Curley S. A. 2003 Combined resection and radiofrequency ablation for advanced hepatic malignancies: results in 172 patients *Ann Surg Oncol* **10** 1059-1069.

Pesavento A., Lorenz A., Siebers S. and Ermert H. 2000 New real-time strain imaging concepts using diagnostic ultrasound *Phys Med Biol* **45** 1423-1435.

Pichardo S., Gelet A., Curiel L., Chesnais S. and Chapelon J. Y. 2008 New integrated imaging high intensity focused ultrasound probe for transrectal prostate cancer treatment *Ultrasound Med Biol* **34** 1105-1116.

Plewes D. B., Bishop J., Samani A. and Sciarretta J. 2000 Visualization and quantification of breast cancer biomechanical properties with magnetic resonance elastography *Phys Med Biol* **45** 1591-1610.

Righetti R., Kallel F., Stafford R. J., Price R. E., Krouskop T. A., Hazle J. D. and Ophir J. 1999 Elastographic characterization of HIFU-induced lesions in canine livers *Ultrasound Med Biol* **25** 1099-1113.

Rivoire M., De Cian F., Meeus P., Negrier S., Sebban H. and Kaemmerlen P. 2002 Combination of neoadjuvant chemotherapy with cryotherapy and surgical resection for the treatment of unresectable liver metastases from colorectal carcinoma *Cancer* **95** 2283-2292.

Souchon R., Rouviere O., Gelet A., Detti V., Srinivasan S., Ophir J. and Chapelon J. Y. 2003 Visualisation of HIFU lesions using elastography of the human prostate in vivo: preliminary results *Ultrasound Med Biol* **29** 1007-1015.

Srinivasan S., Ophir J. and Alam S. K. 2002 Elastographic imaging using staggered strain estimates *Ultrason Imaging* **24** 229-245.

Taylor L. S., Porter B. C., Rubens D. J. and Parker K. J. 2000 Three-dimensional sonoelastography: principles and practices *Phys Med Biol* **45** 1477-1494.

Varghese T., Zagzebski J. A. and Lee F. T. 2002 Elastographic imaging of thermal lesions in the liver in vivo following radiofrequency ablation: preliminary results *Ultrasound Med Biol* **28** 1467-1473.

Varghese T., Zagzebski J. A., Rahko P. and Breburda C. S. 2003 Ultrasonic imaging of myocardial strain using cardiac elastography *Ultrason Imaging* **25** 1-16.

Vykhodtseva N., McDannold N. and Hynynen K. 2006 Induction of apoptosis in vivo in the rabbit brain with focused ultrasound and Optison *Ultrasound Med Biol* **32** 1923-1929.

Wu F., Wang Z. B., Chen W. Z., Zhu H., Bai J., Zou J. Z., Li K. Q., Jin C. B., Xie F. L. and Su H. B. 2004 Extracorporeal high intensity focused ultrasound ablation in the

treatment of patients with large hepatocellular carcinoma *Ann Surg Oncol* **11** 1061-1069.

Zahiri-Azar R. and Salcudean S. E. 2006 Motion estimation in ultrasound images using time domain cross correlation with prior estimates *IEEE Trans Biomed Eng* **53** 1990-2000.

Zhu Y. and Hall T. J. 2002 A modified block matching method for real-time freehand strain imaging *Ultrason Imaging* **24** 161-176.

Figures captions

Figure 1: Schematic diagram of the experimental apparatus.

Figure 2: Relation between sizes measured (A) on pathology and on strain images and (B) on pathology and sonograms. Significant correlation was found in both cases.

Figure 3: Comparison using Student tests of the contrasts measured on sonograms and strain images. Raw data and mean ± standard deviation are shown. The contrast of the entire lesion observed on strain images was significantly higher when compared to the contrast of the entire ablation observed on sonograms ($p<0.05$).

Figure 4: Single ablation produced in 40 seconds using the toroidal HIFU device. (A) Ablation imaged using B-mode imaging (full arrow = 15 mm, doted arrow = 17 mm, contrast = 5.6 dB), (B) corresponding strain image (full arrow = 15 mm, doted arrow = 18 mm, contrast = 22.5 dB, CNRe = 9.3, SNRe = 2.1) and (C) corresponding gross pathology (full arrow = 16 mm, doted arrow = 18 mm).

Figure 5: Strain images have allowed the visualization of veins (in circle) close to the ablated zone (A) and of abscesses (B), black and white representing low (0%) and high (5%) strain, respectively in both images.

Figure 6: In that particular case, only a portion of the HIFU ablation was visible on B-mode images (full arrow = 15 mm, doted arrow = 10 mm, contrast = 1.9 dB) (A). The corresponding strain image (B) (full arrow = 14 mm, doted arrow = 21 mm, contrast = 9.1 dB, CNRe = 1.9, SNRe = 1.8) is more closely related to (C) the actual ablation observed on gross pathology (full arrow = 15 mm, doted arrow = 20 mm) where the HIFU ablation has different appearances, corresponding to a zone where the activity of cavitation and/or ebullition may have been significant (darker area and cavities at the top of the image).

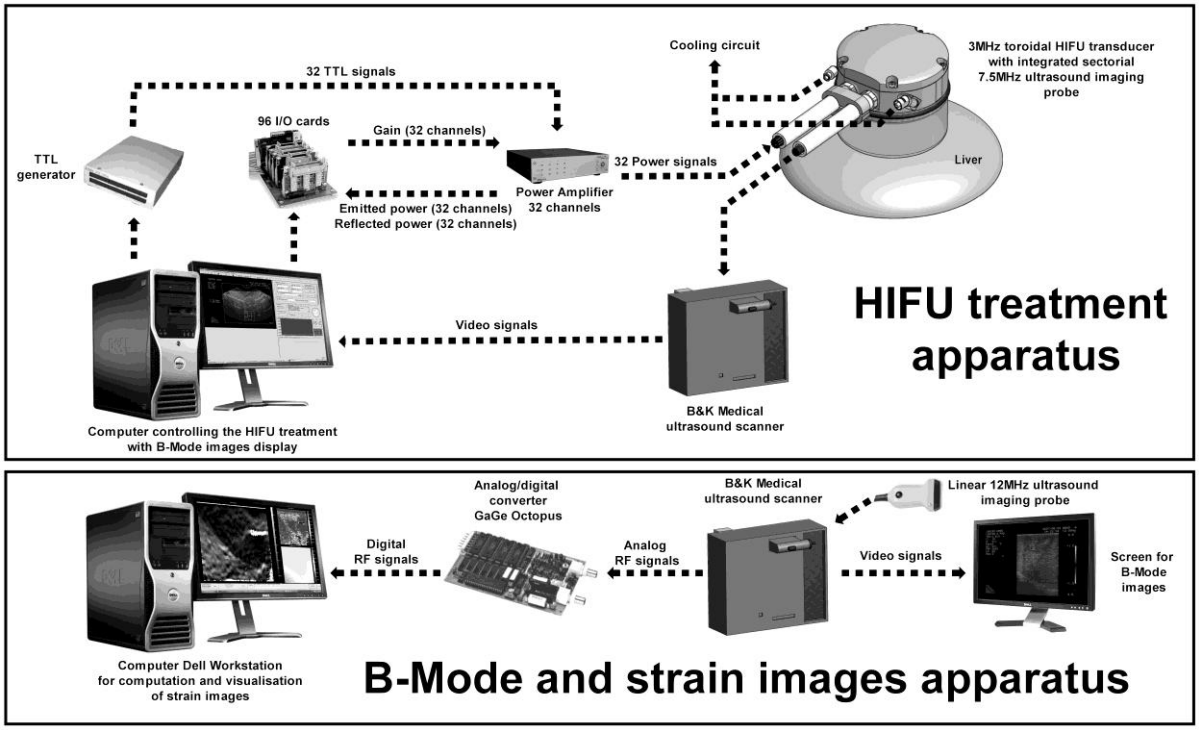
Cooling circuit
3MHz toroidal HIFU transducer with integrated sectorial 7.5MHz ultrasound imaging probe
32 TTL signals
96 I/O cards
Gain (32 channels)
TTL generator
32 Power signals
Liver
Power Amplifier 32 channels
Emitted power (32 channels)
Reflected power (32 channels)
Video signals
HIFU treatment apparatus
Computer controlling the HIFU treatment with B-Mode images display
B&K Medical ultrasound scanner
Analog/digital converter GaGe Octopus
B&K Medical ultrasound scanner
Linear 12MHz ultrasound imaging probe
Digital RF signals
Analog RF signals
Video signals
Screen for B-Mode images
Computer Dell Workstation for computation and visualisation of strain images
B-Mode and strain images apparatus

Figure 1.

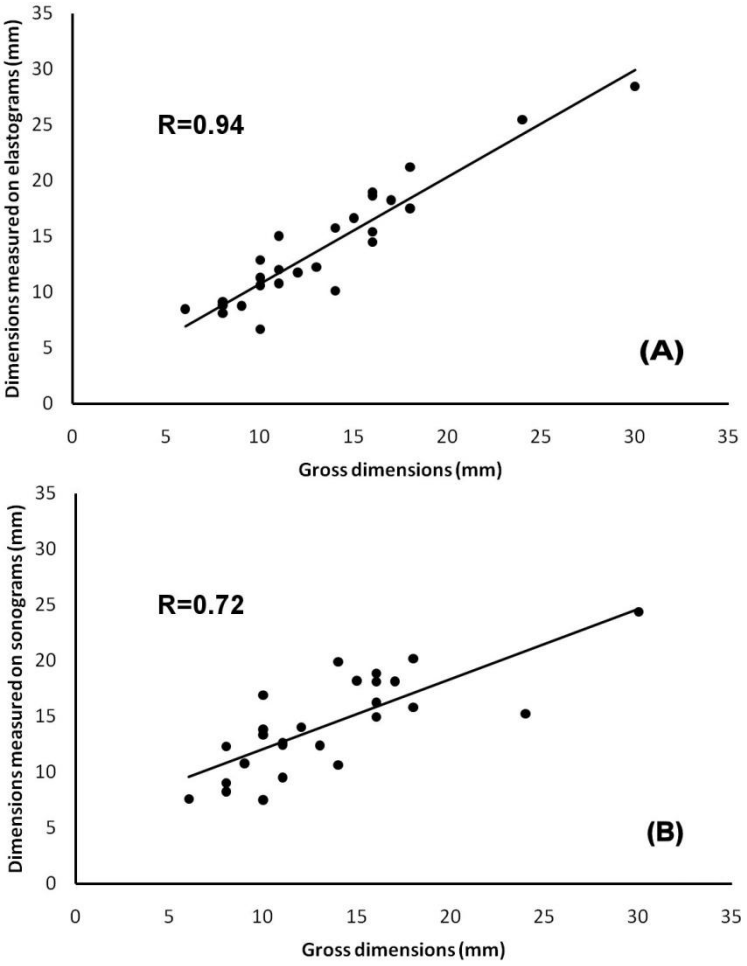
Dimensions measured on elastograms (mm)
R=0.94
(A)
Gross dimensions (mm)
Dimensions measured on sonograms (mm)
R=0.72
(B)
Gross dimensions (mm)

Figure 2.

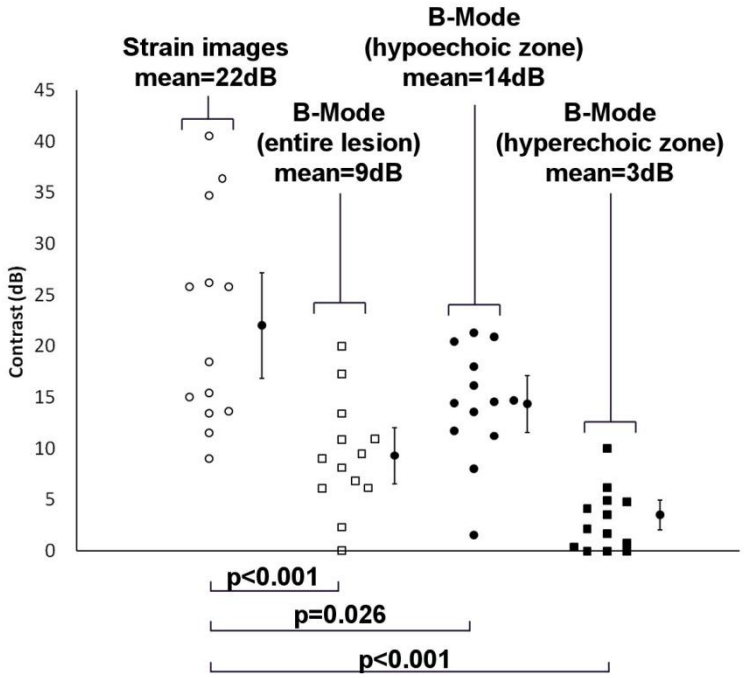
Strain images
mean=22dB
B-Mode
(hypoechoic zone)
mean=14dB
B-Mode
(entire lesion)
mean=9dB
B-Mode
(hyperechoic zone)
mean=3dB
Contrast (dB)
45
40
35
30
25
20
15
10
5
0
p<0.001
p=0.026
p<0.001

Figure 3.

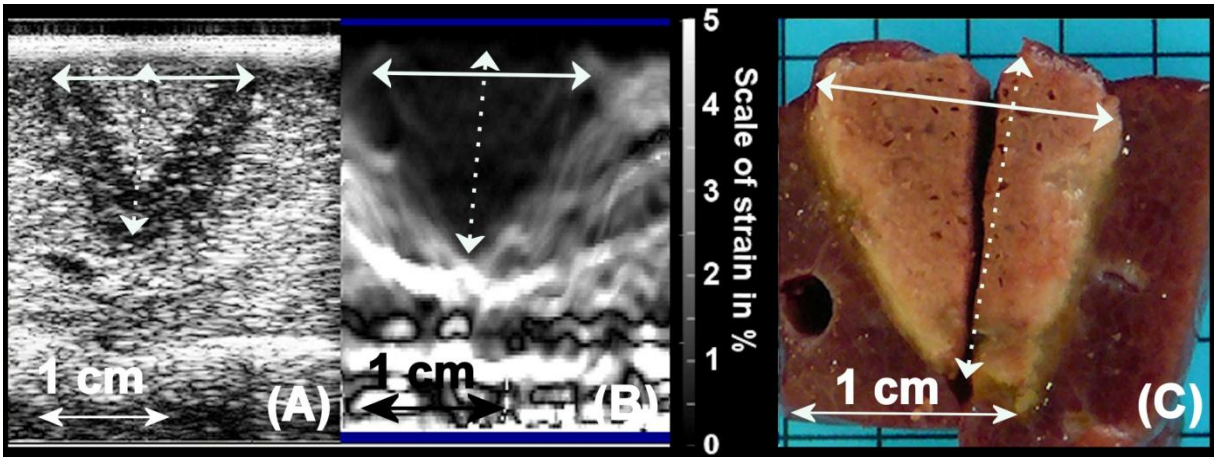

Figure 4.

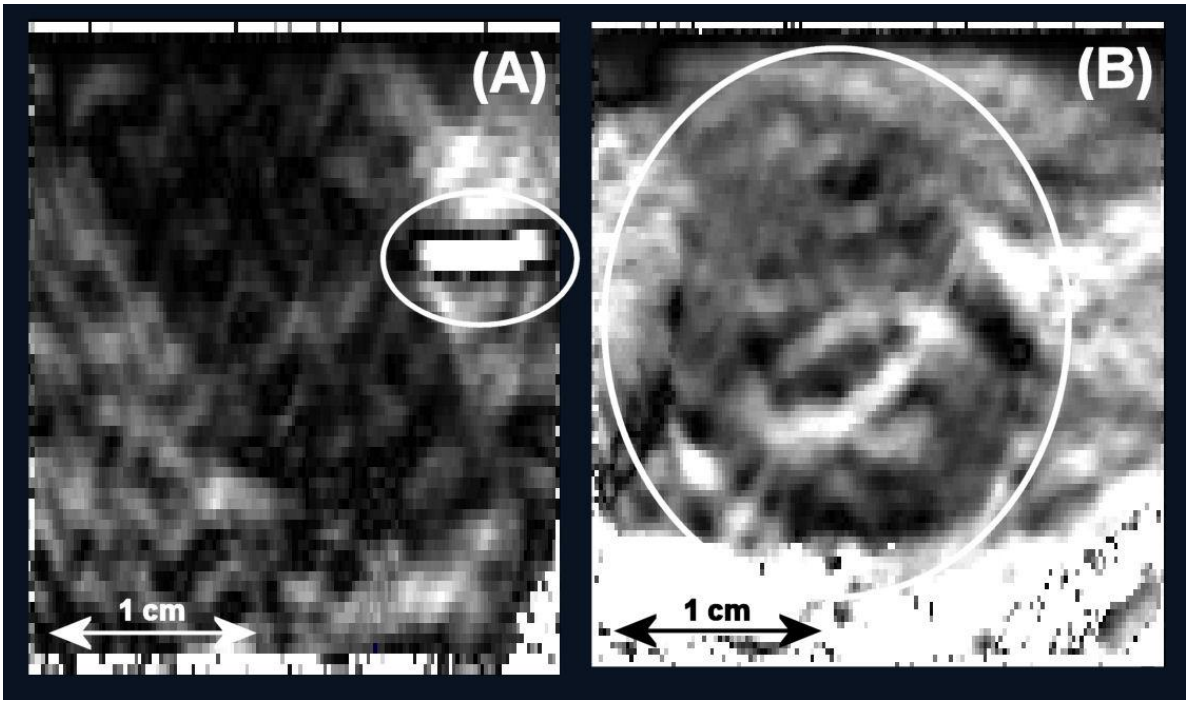

Figure 5.

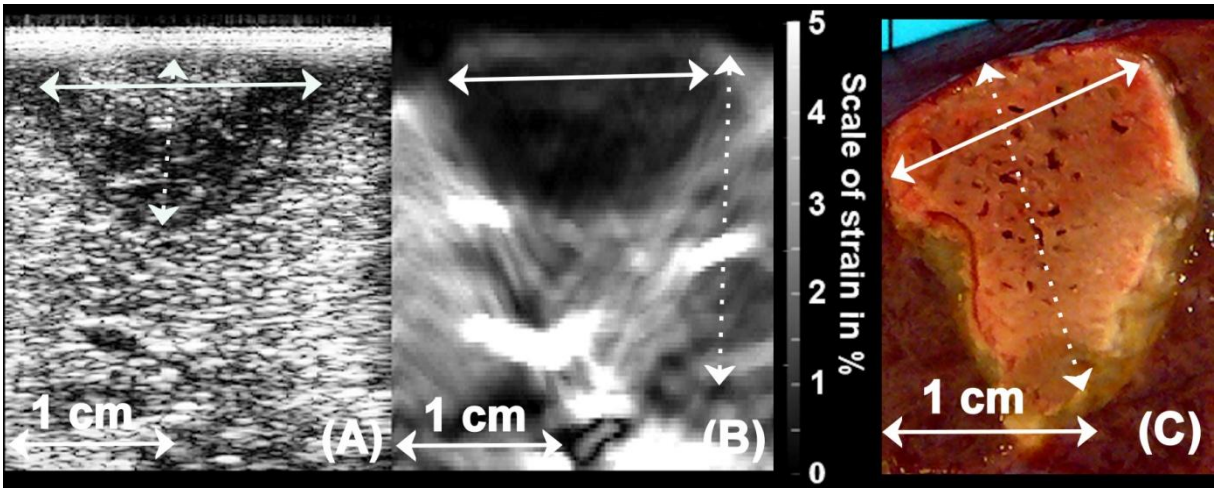

Figure 6.

Table 1: CNRe, SNRe, contrast and dimension measured on elastograms, sonograms and pathology.

		Mean	Standard deviation
Elastography	Contrast (dB)	22.0	10.3
	CNRe	11.4	3.1
	SNRe	2.8	1.1
	Width of the lesion (mm)	12.2	3.9
	Length of the lesion (mm)	16.1	6.1
Sonogram	Contrast of the all lesion (dB)	9.3	5.5
	Contrast of the hyperechoic zone (dB)	3.5	3.0
	Contrast of the hypoechoic zone (dB)	14.4	5.5
	Width of the lesion (mm)	13.5	4.0
	Length of the lesion (mm)	15.1	4.7
Pathology	Width of the lesion (mm)	11.4	3.3
	Length of the lesion (mm)	15.6	6.2